Limitations of the Method of Moments for Unlike-Spin Broadening

R. E. Walstedt
Bell Telephone Laboratories, Murray Hill, New Jersey 07974
(Received 24 August 1971)

The magnetic resonance line-shape analysis based on the second and fourth moments of the frequency distribution, as originally formulated by Van Vleck, is shown to give incorrect results in the presence of the combined conditions (a) rapidly modulated (i.e., narrowed) interactions with unlike-spin species and (b) like-spin broadening comparable to (or greater than) that from mechanism (a). A new line-shape analysis is given based on density-matrix perturbation theory which specifically treats the case of rapidly modulated unlike-spin coupling. The results are compared with the moment analysis and applied to several examples from the literature. The case of the ^{19}F NMR linewidth in antiferromagnetic MnF_2 is discussed in considerable detail, including a detailed evaluation of the ^{19}F-^{19}F Suhl-Nakamura coupling. Experimental results are reported for the inhomogeneous ^{19}F line broadening in a MnF_2 crystal of excellent quality, allowing a comparison of measured and calculated free-induction decay times. Contrary to the earlier "method-of-moments" analysis, in which the ^{19}F line was thought to be narrowed by the combined effect of ^{19}F-^{55}Mn dipolar coupling and ^{55}Mn-^{55}Mn Suhl-Nakamura interaction, we find the linewidth to be accounted for by ^{19}F-^{19}F spin-spin interactions alone. This conclusion is in agreement with the new line-shape theory.

I. INTRODUCTION

In nuclear-magnetic-resonance (NMR) studies there frequently arises the question of the effect of nonresonant or "unlike" nuclear species on the width and shape of an observed resonance line. Such effects have traditionally been discussed in terms of moments of the line-shape function as expounded in the classic treatment by Van Vleck.[1] There it is pointed out that strong interactions among unlike spins can lead to line-narrowing effects if they make a large contribution to the fourth moment M_4 such that the ratio $\epsilon = M_4/M_2^2 \gg 3$. In such a case the line shape is predicted to be a Lorentzian of width

$$\langle \Delta\omega \rangle \sim \epsilon^{-1/2} M_2^{1/2} \ll M_2^{1/2} . \quad (1)$$

Clear-cut examples of this phenomenon have been reported by Abragam and Winter[2] for the compounds AgF and KF, where the relatively larger dipole interactions among the ^{19}F nuclei lead to considerable narrowing of the silver and potassium NMR lines.

There is, however, a range of cases where application of the above moment criterion leads to incorrect results. This occurs when the Lorentzian width [Eq. (1)] is of the order of or less than the expected width *from like-spin interactions alone*. This may be seen by arguing that rapid motion of unlike spins can in no way average out (i.e., narrow) the couplings between the resonant nuclei. As unlike-spin motion increases, then, the line will necessarily approach the width and shape determined by the like-spin interactions regardless of the *total* moment values involved. In this limit (1) will underestimate the true width, and the line will not, in general, have the predicted Lorentzian shape.

This difficulty occurs only in the case of rapidly modulated unlike-spin couplings. It is closely related to line broadening by spin-lattice interactions, where one would not usually attempt to apply the moment analysis. As is well known,[3] line shapes are unaffected by weak spin-lattice interactions, independent of what "moment" contributions they might make.

The purpose of this paper is to examine the unlike-spin line-broadening problem in some detail and to present a correct theory. In Sec. II, we summarize the basic results from the moment method in the case of two spin species and illustrate further the limit in which this scheme breaks down. In Sec. III, density-matrix perturbation theory is employed to give a line-shape analysis which is valid specifically for rapidly modulated unlike-spin couplings. The results of Ref. 2 are reexamined in terms of the new results.

In Sec. IV, the new line-shape theory is applied to the case of the ^{19}F linewidth in antiferromagnetic MnF_2. This resonance is an excellent example of the difficulty with Eq. (1), in that the very strong Suhl-Nakamura[4,5] coupling between the ^{55}Mn nuclei makes a major contribution to the fourth moment via the ^{19}F-^{55}Mn dipolar coupling. In the traditional moment picture, then, the ^{19}F resonance *appears* to be strongly narrowed. The new line-shape theory shows, in contrast, that the ^{19}F width is determined almost exclusively by ^{19}F-^{19}F coupling.

One of the principal difficulties in the experimental study of the ^{19}F line shape and width is the sensitivity of the ~40 kG transferred hyperfine field at the ^{19}F nuclei to strains and crystalline imperfec-

tions. Thus virtually no crystals of MnF_2 are available which are totally free from inhomogeneous ^{19}F line broadening. In previous work, then, results of the standard moment analysis have been compared with the measured spin-echo lifetime,[6,7] giving a result more than three times the measured value[6] 29 ± 1 μsec. Quite apart from the question of this disparity it must be remarked that there is no established quantitative connection between spin-echo and (homogeneous) free-induction decay times in solids except for special cases such as $\frac{1}{2}\pi$-π echoes or a strongly narrowed line. For the case of a single species with dipolar and/or Suhl-Nakamura coupling, a preliminary calculation shows the "second moment" of a $\frac{1}{2}\pi$-θ spin-echo decay function[8] to be proportional to $-\cos\theta$. Thus for $\frac{1}{2}\pi$-π echoes M_2 is unchanged, but for $\frac{1}{2}\pi$-$\frac{1}{2}\pi$ echoes it vanishes. This means that the decay of such echoes is governed by higher moments which are generally unfeasible to calculate. We shall see in Sec. IV that the homogeneous free-induction decay time for MnF_2: ^{19}F is considerably shorter than the measured spin-echo lifetime.

To avoid the uncertainties of spin-echo decay, it is desirable to study the homogeneous free-induction decay function. This is made possible by measuring the distribution of inhomogeneous fields in the best available crystal using a strong rf-field technique to be described below. The results of this measurement are then folded into the expected line shape from the analysis of Sec. III, and then Fourier transformed for comparison with the experimental free-induction decay.

Although the ^{19}F-^{19}F spin coupling is predominantly dipolar in character, the Suhl-Nakamura[3,4] (SN) interaction makes a small[7] but non-negligible contribution to the linewidth. This effect has been discussed at length in the literature.[5,7] Nonetheless, because of errors in earlier treatments, we present a detailed account of the ^{19}F SN coupling in Sec. IV and in the Appendix and make a number of observations that have hitherto been passed over.

Finally, in Sec. V, we touch upon the difficult question of spin-echo decay and report some qualitative experimental observations on MnF_2: ^{19}F.

II. MOMENT METHOD FOR UNLIKE-SPIN BROADENING

Here we discuss the moment analysis of line shapes and its limitations, in a context of two interacting unlike-spin systems. These we denote $\vec{I}_i$ and $\vec{S}_i$ with the $\vec{I}_i$ resonant. The spin-spin interaction Hamiltonian is assumed to have the usual form

$$\mathcal{H}_{\rm int} = \mathcal{H}_{II} + \mathcal{H}_{IS} + \mathcal{H}_{SS}, \tag{2}$$

where the subscripts denote the nuclei concerned in an obvious notation. In Eq. (2), we keep only the high-field secular terms, so that $\mathcal{H}_{IS}$ has the simple form

$$\mathcal{H}_{IS} = \sum_{i,j} C_{ij} I_i^z S_j^{z'} . \tag{3}$$

The normalized absorption line-shape function $g_I(\omega)$ is characterized by the moments[9] $M_n^I = \int_{-\infty}^{\infty} d\omega\, \omega^n g(\omega)$. For practical reasons one is usually limited to working with the first two nonzero moments which may be expressed here as

$$M_2^I = M_2^{II} + M_2^{IS},$$
$$M_4^I = M_4^{II,II} + M_4^{II,IS} + M_4^{IS,IS} + M_4^{IS,SS} . \tag{4}$$

The superscripts of M_2^{II} and M_2^{IS} refer to the terms in (2) which generate these contributions. In M_4^I, the superscripts denote the pair of terms in (2) which give rise to each contribution. In terms of the ratio ϵ defined above, the general criterion for Gaussian-like or Lorentzian-like line shapes becomes $\epsilon \sim 3$ (Gaussian) and $\epsilon \gg 3$ (Lorentzian). In the latter case the linewidth is given approximately by (1) in the original formulation of this technique. The circumstances under which this procedure breaks down, as described above, may be expressed as

$$M_4^{IS,SS} \gg M_4^{II,II},\ M_4^{IS,IS}, \tag{5a}$$
$$\epsilon \gg 3, \tag{5b}$$
$$(M_2^{IS})^{3/2} (M_4^{IS,SS})^{-1/2} \lesssim (M_2^{II})^{1/2}, \tag{5c}$$

where (5a) signifies a case of rapidly modulated interaction with unlike spins, (5b) has traditionally indicated that the line is narrowed to a width

$$\langle \Delta\omega \rangle \sim (M_2^{II} + M_2^{IS})^{3/2} (M_4^{IS,SS})^{-1/2}, \tag{6}$$

and (5c) characterizes the linewidth given in (6) as being relatively small so that $\langle \Delta\omega \rangle < (M_2^{II})^{1/2}$. The essential difficulty here may be seen by arguing that since $[\mathcal{H}_{II}, \mathcal{H}_{SS}] = 0$, the rapid motion represented by $\mathcal{H}_{SS}$ cannot "average out" the I-I coupling. In no case, then, can the linewidth be less than the "I-spin-only" value $(M_2^{II})^{1/2}$, in contradiction with the method-of-moments result (6). In other words, the $\mathcal{H}_{IS}$ broadening can be narrowed by $\mathcal{H}_{SS}$, but $\mathcal{H}_{II}$ broadening cannot.

Although in NMR studies the moments analysis is usually applied to nuclear-nuclear coupling phenomena, a familiar example of conditions (5) is provided by line broadening due to spin-lattice interactions. Consider specifically the cases of relaxation to conduction-electron spins in a metal or to a system of atomic moments in an exchange-coupled paramagnet. These spins then become the S system in the above formulation. The hyperfine coupling operators in such systems would make enormous contributions in a second-moment calcu-

lation, so that the nuclear spin-spin term M_2^{II} would be completely overshadowed in Eq. (6). On the other hand, such interactions are strongly narrowed by the kinetic and exchange fluctuations, respectively, as expressed by conditions (5a) and (5b).[10] In the frequently encountered case that lifetime (T_1) broadening is weak [i.e., condition (5c)], the line shape is well known to be determined by the spin-spin couplings $\mathcal{H}_{II}$ alone.

It is clear, then, that Eq. (6) must be abandoned for an approach in which the effects of $\mathcal{H}_{II}$ and $\mathcal{H}_{IS}$ are treated independently. In the limit $\epsilon \to \infty$, the line shape must reduce to that obtained from $\mathcal{H}_{II}$ alone, and in the limit of strong "lifetime" broadening the line must become Lorentzian with a width given approximately by $(M_2^{IS})^{3/2}(M_4^{IS-SS})^{-1/2}$. In Sec. III, we present a density-matrix perturbation calculation which meets these requirements.

III. DENSITY-MATRIX PERTURBATION TREATMENT

We now apply the highly developed[11] density-matrix perturbation methods to the calculation of the I-spin free-induction decay function $f_I(t)$, given the Hamiltonian (2) and the assumption that $\mathcal{H}_{IS}$ is rapidly modulated by $\mathcal{H}_{SS}$. We begin with the density-matrix equation of motion $i\dot{\rho} = [\mathcal{H}, \rho]$. This is transformed to an interaction representation using

$$\rho' = T\rho T^{+} ,$$

where[12]

$$T = \exp[i(\mathcal{H}_{SS} - \omega_I \textstyle\sum_i I_i^z - \omega_S \sum_j S_j^{z'})t] .$$

T takes the system into a rotating frame for the I spins, i.e., it removes the oscillatory part of the free-induction process; it also introduces explicitly the time modulation of $\mathcal{H}_{IS}$: $\mathcal{H}_{IS}(t) = e^{i\mathcal{H}_{SS}t}\mathcal{H}_{IS}e^{-i\mathcal{H}_{SS}t}$. The equation of motion then becomes

$$i\dot{\rho}' = [\mathcal{H}_{II}, \rho'] + [\mathcal{H}_{IS}(t), \rho'] . \tag{7}$$

Our procedure is to develop the second term in (7) to second order in $\mathcal{H}_{IS}$ as in the standard treatment of stationary random perturbations.[11] The first term is left in exact form. It is convenient in the high-temperature limit to approximate the state of the S nuclei by one of infinite spin temperature since the corrections to this zero-order picture are generally very small. Thus we take

$$\rho'(t) \cong \rho_I(t) \times 1_S/\mathrm{Tr}(1_S) , \tag{8}$$

where 1_S is the unit matrix of the S manifold and $\rho_I(t)$ is defined in the I manifold. Next we integrate (7) from 0 to t giving

$$\rho'(t) = \rho'(0) - i\int_0^t dt' \,[\mathcal{H}_{II}, \rho'(t')] - i\int_0^t dt' \,[\mathcal{H}_{IS}(t'), \rho'(t')].$$

We substitute this equation for $\rho'(t)$ into the second term of (7), and take the trace over the S manifold (Tr_S), finding

$$\dot{\rho}_I(t) = -i[\mathcal{H}_{II}, \rho_I(t)] - \mathrm{Tr}_S \int_0^t dt' \,[\mathcal{H}_{IS}(t), [\mathcal{H}_{IS}(t'), \rho'(t')]] . \tag{9}$$

Two terms have vanished with Tr_S, a consequence of our neglect of correlations between $\mathcal{H}_{IS}(t)$ and $\rho'(t)$ as embodied in (8).

We specialize (9) to the study of transverse magnetization $\langle I^x \rangle$ by multiplying both sides by I^x and taking Tr_I. Using (8) and (3) the $S_i^{z'}$ operators can be extracted from the double commutator in (9) to give

$$\frac{d}{dt}\mathrm{Tr}[I^x\rho_I(t)] = -i\,\mathrm{Tr}\{I^x[\mathcal{H}_{II}, \rho_I(t)]\} - \tfrac{1}{3}S(S+1) \times \sum_j C_{ij}^2 \int_0^t d\tau\, a(\tau)\,\mathrm{Tr}[I^x\rho_I(t-\tau)] , \tag{10}$$

where we have introduced the autocorrelation function of $\mathcal{H}_{IS}$:

$$a(\tau) = \mathrm{Tr}[\mathcal{H}_{IS}(\tau)\mathcal{H}_{IS}]/\mathrm{Tr}(\mathcal{H}_{IS}^2) . \tag{11}$$

The central assumption of the calculation, that of rapid modulation of $\mathcal{H}_{IS}(t)$, is now employed in (10) to remove $\mathrm{Tr}[I^x\rho_I(t-\tau)] \cong \mathrm{Tr}[I^x\rho_I(t)]$ from the τ integral. Thus we assume the correlation time $\tau_c = \int_0^\infty d\tau\, a(\tau)$ to be short enough so that the change of $\mathrm{Tr}[I^x\rho_I(t)]$ can be neglected over this interval. Put another way, $\tau_c \ll T_2$, where T_2 is the composite transverse relaxation time. By the same argument we extend the integration limit in (10) to infinity. The equation governing transverse relaxation becomes finally

$$\frac{d}{dt}\mathrm{Tr}(I^x\rho_I) = -i\,\mathrm{Tr}\{I^x[\mathcal{H}_{II}, \rho_I]\} - \mathrm{Tr}(I^x\rho_I)/T_2^{IS} . \tag{12}$$

$1/T_2^{IS}$, the transverse relaxation rate due to unlike spins alone, is defined as

$$1/T_2^{IS} = \tfrac{1}{3}S(S+1)\tau_c \textstyle\sum_j C_{ij}^2 . \tag{13}$$

Equation (12) is seen to be satisfied by taking $\rho_I(t) = e^{-t/T_2^{IS}} e^{-i\mathcal{H}_{II}t}\,\rho_I(0)e^{i\mathcal{H}_{II}t}$, whereupon $\mathrm{Tr}[I^x\rho_I(t)]$ becomes simply the product of free-induction functions for like-spin and unlike-spin relaxation processes taken separately.

In the high-temperature limit, the free-induction function becomes

$$f_I(t) = f_{II}(t)\, e^{-t/T_2^{IS}} , \tag{14}$$

where

$$f_{II}(t) = \mathrm{Tr}(I^x e^{-i\mathcal{H}_{II}t} I^x e^{i\mathcal{H}_{II}t})/\mathrm{Tr}(I^x)^2 \qquad (15)$$

is the rigorous free-induction function for I spins alone. In the approximations employed here, then, the two contributions to free-induction decay act essentially independently.[13]

Using the fundamental Fourier-transform relation[9] between free-induction and line-shape functions, the latter is easily shown to be the convolution

$$g_I(\omega) = \int_{-\infty}^{\infty} \frac{d\omega' g_{II}(\omega') T_2^{IS}/\pi}{1+(\omega-\omega')^2 (T_2^{IS})^2} , \qquad (16)$$

where $g_{II}(\omega)$ corresponds to $f_{II}(t)$. As written, the moments M_2^I and M_4^I of (16) diverge. This is only a minor defect, however, and will be corrected by allowing the Lorentzian in (16) to be terminated in suitable fashion at frequencies of the order of $\omega - \omega' = \pm \tau_c^{-1}$. The short-correlation-time approximation, which says that τ_c^{-1} is much greater than the linewidth, allows these corrections to be neglected in (16).

In the light of Eq. (16), we discuss now various cases of relative like- and unlike-spin broadening with reference to the moment analysis as discussed earlier:

(a) Assigning a suitable relaxation time T_2^{II} to $f_{II}(t)$ [Eq. (15)], we see that for $T_2^{IS} \ll T_2^{II}$ [the opposite of (5c)] the Lorentzian width dominates (16), and the unmodified moment analysis gives an approximately correct linewidth [Eq. (6)].

(b) In the opposite limit $T_2^{II} \ll T_2^{IS}$ the Lorentzian in (16) becomes essentially a δ function, and we find $g_I(\omega) \cong g_{II}(\omega)$. For this case the moment picture is applicable but must be altered to the extent of excluding all but the initial terms in Eqs. (4). In other words, the unlike-spin couplings may simply be ignored. This was the conclusion in the spin-lattice relaxation examples of Sec. II. By making the correspondence $T_2^{IS} \to T_1$ we obtain in this case the condition $T_2 \ll T_1$ encountered in the earlier discussion. In this connection we note that the procedure for obtaining the basic equation (12) goes through essentially unchanged in the case that $\mathcal{H}_{IS}$ is a spin-lattice coupling operator.

(c) In the intermediate case $T_2^{IS} \sim T_2^{II}$ we find no applicable counterpart in the moment method. When $g_{II}(\omega)$ is a Gaussian, we obtain the complicated transition region between Gaussian and Lorentzian line shape. In the opposite case of Lorentzian shape for $g_{II}(\omega)$, one has $f_{II}(t) = e^{-t/T_2^{II}}$, and from (14) and (16) it follows that the combined effect produces a Lorentzian line of width $1/T_2^{II} + 1/T_2^{IS}$. This behavior has been observed in the case of the exchange-narrowed ^{195}Pt NMR line in Pt metal.[14,15]

Let us now apply the above results to the examples from the literature quoted in the Introduction. In the NMR studies of AgF and KF[2] the ^{109}Ag and ^{39}K linewidths were estimated including only the unlike-spin contribution $1/T_2^{IS}$. We shall see that these resonances are examples of the intermediate case (c) above, though not dramatic ones. The relevant moment parameters for these cases taken from Ref. 2 are summarized in Table I. In addition, the small second-moment contributions M_2^{II} have been calculated and are also given in the table. All entries are in the notation of Sec. II. In each case M_2^{II} is seen to be well less than 1% of M_2^{IS}, yet the like-spin-only linewidth contribution $(M_2^{II})^{1/2}/\gamma_I$ is found to be of the same order as the strongly narrowed unlike-spin part. The latter was estimated[2] with a truncated-Lorentzian (TL) model line shape.

On the basis of Eq. (16) it is suggested that the linewidth contributions $1/\gamma_I T_2^{IS}$ and $(M_2^{II})^{1/2}/\gamma_I$ in Table I should be combined in some fashion for comparison with the experimental linewidth shown on the bottom line. In the case of AgF simple addition of these contributions gives improved agreement with experiment, but the change is well within the error limits. For KF, however, the like-spin contribution results in considerably better agreement with experiment, though not enough to account for the total discrepancy. In this connection we note that the truncated-Lorentzian model has been found in some cases to underestimate NMR linewidths.[16] Nonetheless, these cases illustrate how effective a very small second-moment contribution from like spins can be in broadening a line where ϵ is large.

IV. LINEWIDTH OF ^{19}F IN ANTIFERROMAGNETIC MnF_2

Our main example, that of the zero-temperature ^{19}F linewidth in MnF_2, is one of considerably greater complexity (a) because the $\mathcal{H}_{SS}$ (^{55}Mn-^{55}Mn) and $\mathcal{H}_{II}$ (^{19}F-^{19}F) interaction terms both include the combined effects of dipolar and Suhl-Nakamura energies and (b) because the ^{19}F NMR line (in zero field) actually consists of two resonances with fre-

TABLE I. Moment and linewidth parameters for the resonances indicated. All but the quantity M_2^{II} are taken from Ref. 2.

	^{109}Ag in AgF	^{39}K in KF
M_2^{II}/γ_I^2	0.004 16 G^2	0.0163 G^2
M_2^{IS}/γ_I^2	4.19 G^2	2.54 G^2
ϵ	57	57
$1/\gamma_I T_2^{IS}$(TL)	0.235 G	0.192 G
$(M_2^{II})^{1/2}/\gamma_I$	0.064 G	0.13 G
Experimental half-width	0.3 ± 0.15 G	0.5 ± 0.05 G

TABLE II. Calculated moments of the low-temperature ^{19}F NMR in MnF_2.

	Moment	Calculated value
	M_4^{IS-SS} [a]	1.8×10^{21} sec^{-4}
	M_2^{IS} [b]	2.7×10^{9} sec^{-2}
Terms in M_2^{II}	M_2^{II} (dipole) [b]	2.9×10^{9} sec^{-2}
	M_2^{II} (dipole-SN) [c]	-5×10^{8} sec^{-2}
	M_2^{II} (SN) [c]	1.9×10^{9} sec^{-2}
	$M_2^{II'}(zz)$ [b]	0.74×10^{8} sec^{-2}
	$M_2^{II'}(\pm\pm)$ [d]	1.47×10^{9} sec^{-2}
(Sum)	M_2^{II}	5.8×10^{9} sec^{-2}

[a]Reference 7. [c]This work.
[b]References 5 and 17. [d]Reference 17.

quencies equal in magnitude but opposite in sign. The latter circumstance leads us to consider the ^{19}F resonance to consist of two quasi-"unlike" species I and I', differing from ordinary unlike species in that coupling terms of the form $I^{\pm}I'^{\pm}$ conserve Zeeman energy and must be included[17] in moment calculations.

A. Moments of ^{19}F Line Shape

Calculated values of M_2^{IS} and M_4^{IS-SS} are given in Table II as well as M_2^{II} and its various contributions. We discuss briefly the origin of each entry in the table, with a detailed discussion of the Suhl-Nakamura coupling contributions given in the Appendix.

M_2^{IS} is obtained from a purely dipolar term [Eq. (3)], with the value quoted taken from Refs. 5 and 17.

M_4^{IS-SS} represents the cross term between dipolar coupling [Eq. (3)] and the very large Suhl-Nakamura coupling among ^{55}Mn nuclei, and is by far the largest contribution to M_4^I in Eq. (4). This term has been calculated in detail by Hone *et al.*[7]; their value is adopted here.

Of the various contributions to M_2^{II}, the terms M_2^{II} (dipole) and $M_2^{II'}(zz)$ come from purely dipolar interactions, where the superscripts II and II' denote coupling between like and unlike ^{19}F's, respectively. The values of these terms given in Refs. 5 and 17 are again adopted here.

The Suhl-Nakamura term M_2^{II} (SN) and the SN-dipolar interference term M_2^{II} (dipole-SN) are calculated in the Appendix. M_2^{II} (SN) for MnF_2:^{19}F has been discussed at some length in the literature.[5,7] Hone *et al.*[7] corrected an error in sign in Ref. 5, reducing the original estimate of M_2^{II} (SN) by more than an order of magnitude. Here we correct another minor point in this calculation which was overlooked in previous work. Because of the low symmetry of the F^- sites in MnF_2 there are ^{19}F-^{19}F SN coupling coefficients of two essentially different forms, only one of which was treated in Refs. 5 and 7. The second one is derived in the Appendix, and the second-moment contributions of both are evaluated using the tabulated Green's function for the bcc lattice given by Walker *et al.*[18] Where comparable, the numerical results agree with those of Hone *et al.*[7] within ~ 10%. It is also interesting to note that the ^{19}F-^{19}F SN coupling coefficients vary in quite a disorderly fashion over nearby sites, giving rise to a preponderant contribution to M_2^{II} (SN) from just a few nuclei. Thus the multiple ^{19}F hyperfine coupling in this compound effectively destroys the long-range character of the SN interaction.

The term $M_2^{II'}$ $(\pm\pm)$ arises from interaction terms of the form $I_i^{\pm}I_j'^{\pm}$. Because of the anisotropy of the ^{19}F hyperfine coupling,[19] there are indirect (SN) interaction terms of this form (see Appendix) in addition to the usual dipolar contribution. Because of an accidental cancellation of coefficients, the SN terms are relatively small in MnF_2. However, this unlike-spin indirect-coupling effect is potentially of interest in other antiferromagnetic materials. For our present purpose we adopt the dipolar moment term $M_2^{II'}$ $(\pm\pm)$ calculated by Paquette *et al.*[17] for the nearly identical crystal FeF_2.

One can see immediately from the moments in Table II that the ^{19}F resonance is an example of case (b) from Sec. III, i.e., $T_2^{II} \ll T_2^{IS}$. To estimate T_2^{IS} we use instead of (13) the truncated-Lorentzian approximation

$$1/T_2^{IS} \cong \tfrac{1}{6}\sqrt{3}\,\pi (M_2^{IS})^{3/2}(M_4^{IS-SS})^{-1/2},$$

which yields

$$T_2^{IS} \cong 330\ \mu\text{sec}. \tag{17}$$

The Gaussian approximation $T_2^{II} = \sqrt{2}\,(M_2^{II})^{-1/2}$ to the line shape generated by $\mathcal{H}_{II}$ alone gives $T_2^{II} = 18.7$ μsec. T_2^{IS} therefore makes a contribution of only a few percent to the decay rate, and the observed linewidth should be essentially accounted for by $\mathcal{H}_{II}$ alone. In other words, one can all but ignore the presence of the ^{55}Mn nuclei.

B. Measurement of Inhomogeneous Broadening and Free-Induction Decay

In order to make a comparison of the calculated moment M_2^{II} with the free-induction decay function, the inhomogeneous broadening of the sample has been measured using a technique of pulsed strong rf fields. The technique, which is described in detail by Abragam,[20] consists of measuring the nuclear magnetization following a pulse of applied rf field H_1 at a frequency ω in the vicinity of the resonance frequency ω_0. The rf pulse must be long enough for equilibrium to be reached in the rotating

frame but short compared with T_1. For a square pulse, thermodynamic arguments give a ratio of final to initial magnetization:

$$\frac{M_f}{M_0}=\frac{\Delta H^2}{\Delta H^2+H_1^2+H_L'^2}\ , \tag{18}$$

where $\Delta H=(\omega-\omega_0)/\gamma$ is the distance in field from exact resonance and H_L' is the spin-spin interaction local field to be derived from $\mathcal{H}_{II}$ by $H_L'^2=\mathrm{Tr}(\mathcal{H}_{II}^2)/\gamma^2\mathrm{Tr}(I_z+I_z')^2$. Equation (18) is seen to be an inverted Lorentzian, varying from a value of unity for $\Delta H \to \pm\infty$ to zero at the center of the resonance. The function given applies, of course, only to a perfectly homogeneous resonance line.

The effect of inhomogeneity is included in the analysis by convolving (18) with a normalized distribution $g(h)$ of fields ω_0/γ, which we take for convenience to be centered at $h=0$. The reduced magnetization $m(\Delta H)=M_f/M_0$ then becomes

$$m(\Delta H)=\int_{-\infty}^{\infty}\frac{g(h)\,(\Delta H-h)^2}{(\Delta H-h)^2+H_1^2+H_L'^2}\,dh\ . \tag{19}$$

The response function (19) differs from (18) in that it is broader and no longer falls to zero at $\Delta H=0$. As we shall see, $m(0)$ is a rough measure of the fractional inhomogeneous broadening. With respect to (19), we remark that this result is only valid for the assumed condition of reasonably long-range inhomogeneities. Second, it must be said that the entire procedure is only meaningful for a comparison with the calculated M_2^{II} if the inhomogeneous broadening is a relatively minor effect.

In applying this technique to the measurement of inhomogeneous broadening for MnF_2: ^{19}F, there is a complication due to the presence of the ^{55}Mn spins which must be dealt with rather carefully. In the thermodynamic picture in which (18) is derived the latter nuclei constitute a very large energy reservoir to which the ^{19}F's are coupled with a time constant of the order of T_2^{IS}. Thus, as the rf pulse length t_w is varied, the magnetization first comes to quasiequilibrium near the value in (19), then decays eventually to (essentially) zero.

The measured decay function m vs t_w at a frequency near line center is shown in Fig. 1. It is seen that the rf field is small enough so that the initial decay toward equilibrium is very nearly exponential. The associated saturation time constant τ_{sat} is given roughly by $\tau_{sat}^{-1}\sim\gamma^2H_1^2T_2^{II}$. Following the decay of this initial transient the magnetization is given by $m(\Delta H)\,e^{-t_w/\tau^{IS}}$, where τ^{IS} is the ^{19}F-^{55}Mn coupling time constant. The desired measurement of $m(\Delta H)$ is obtained, then, by extrapolating the data for $t_w>\tau_{sat}$ back to $t_w=0$. The data in Fig. 1 are fitted to a double exponential form

$$m(t_w)=[1-m(\Delta H)]\,e^{-t_w/\tau_{sat}}+m(\Delta H)\,e^{-t_w/\tau^{IS}}\ .$$

This is seen to give a good account of the data, yielding $\tau_{sat}=63\pm5$ μsec, $\tau^{IS}=1.1\pm0.2$ msec, and $m(\Delta H)=0.36\pm0.05$. With the approximate expression above for τ_{sat} we find $H_1\sim1.2$ G. The measured value of τ^{IS} is conveniently long,[21] since the analysis is seriously impaired if $\tau_{sat}\sim\tau^{IS}$. τ_{sat} could not, in our case, be made arbitrarily short because of limited rf power available for rf pulses of this length. In any case, $\tau_{sat}\gtrsim T_2^{II}$ even for

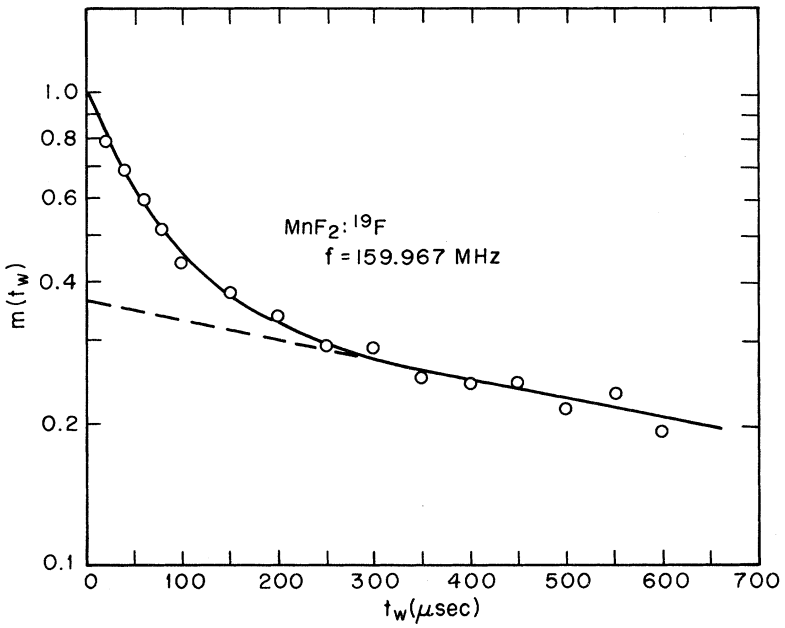

FIG. 1 Reduced ^{19}F nuclear magnetization following the application of a square rf pulse of amplitude H_1 as a function of the length t_w. Pulse frequency given is very near the line center (4.2 °K). Solid curve is fitted to the data as described in the text, the dashed line showing the extrapolation to $m(\Delta H)$ at $t_w=0$.

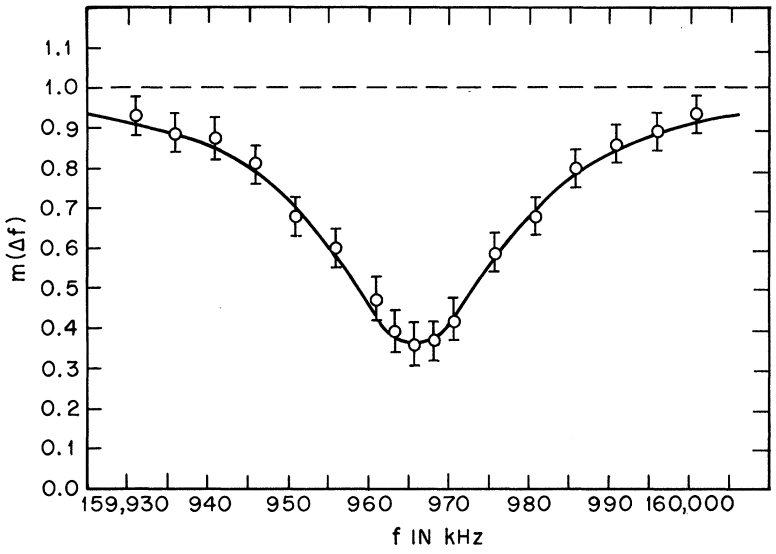

FIG. 2. Measure response function [Eq. (19)] for ^{19}F in MnF_2 at 4.2 °K. Solid line is the evaluation of Eq. (19) using Lorentzian model function for $\mathcal{J}(h)$, fitted to the data. Fit parameters are center, 159 966 kHz; half-width, 14 kHz; minimum, $m(0) = 0.36$.

$\gamma H_1 T_2^{II} > 1$.

With the above procedures, then, an experimental plot of $m(\Delta H)$ vs ΔH was obtained as shown in Fig. 2. The measurement was carried out at 4.2 °K. The function $m(\Delta H)$ is centered at 159.966 ± 0.001 MHz, in excellent agreement with the frequency data of Jaccarino and Walker.[22] The minimum value $m(0) = 0.36$ characterizes the inhomogeneous broadening as appreciable, but not unmanageably large. In order to fit the data of Fig. 2 with Eq. (19) we consider primarily the case of a Lorentzian distribution for $g(h)$. This is the most likely possibility in the event of long-range inhomogeneities due to dilute imperfections.[23] We also consider the case of Gaussian $g(h)$, but not in full detail because a machine calculation is required. With $g(h) = \pi^{-1} H_I (h^2 + H_I^2)^{-1}$, (19) becomes

$$m(\Delta H)\big|_{\text{Lor}} = 1 - \frac{H_D(H_D + H_I)}{(H_D + H_I)^2 + \Delta H^2} \ , \qquad (20)$$

where $H_D^2 = H_1^2 + H_L'^2$ is the "dynamic" contribution to the response width. The total width $H_D + H_I$ is simply the sum of dynamic and inhomogeneous widths. Equation (20) has been fitted to the data of Fig. 2 as shown with excellent results. The width $H_I + H_D = 3.50$ G ± 10% and amplitude at center $H_I/(H_I + H_D) = 0.36 \pm 0.05$ give $H_D = 2.24$ G, and $H_I = 1.25$ G.

H_D may be compared with a calculated H_L' which can be shown to be

$$\gamma^2 H_L'^2 = \tfrac{1}{3} M_2^{II}(\text{dipole}) + \tfrac{1}{3} M_2^{II}(\text{dipole-SN}) + M_2^{II}(\text{SN}) + \tfrac{1}{2} M_2^{II'}(zz) + M_2^{II'}(\pm\pm) \ . \qquad (21)$$

Inserting the numbers from Table II we find $H_L' = 2.5$ G, somewhat larger than the experimental value ($H_L' \cong 2.0$ G) which results when the estimated H_1 contribution is subtracted from the measured H_D. We note that the local field in (21) is more sensitive than the total second moment to the terms $M_2^{II}(\text{SN})$ and $M_2^{II'}(\pm\pm)$, these terms making up 80% of the calculated $H_L'^2$. The discrepancy we find is only slightly outside experimental error but suggests that calculated values of the above-mentioned terms may be too large. In particular, the SN interference effect in $M_2^{II'}(\pm\pm)$ may be more important than suggested in Sec. IV A (see Appendix), since the relevant parameters for the actual case of antiferromagnetic MnF_2 are not available.

Finally, we compare our measured free-induction function with a calculated model function based on M_2^{II} (Table II) and the measured inhomogeneity parameter H_I. Under the assumption of long-range inhomogeneity it is straightforward to show that the observed free-induction signal will have the form

$$f_{\text{obs}}(t) = f_{II}(t) \int_{-\infty}^{\infty} d\omega\, g(\omega) \cos\omega t \ , \qquad (22)$$

where $g(\omega)$ is the ω-space counterpart of $g(h)$. With the Lorentzian distribution $g(h)$ discussed above and a Gaussian model for the preponderantly dipolar homogeneous line, (22) becomes

$$f_{\text{obs}}(t) \cong \exp(-\gamma H_I t - \tfrac{1}{2} M_2^{II} t^2) \ . \qquad (23)$$

The free-induction-signal data are shown in a semilogarithmic plot against t^2 in Fig. 3. Equation (23) is also plotted with the parameter values determined above [$T_2^{II} = 18.7$ μsec, $T_2(\text{inhomo}) = (\gamma H_I)^{-1} = 31.5$ μsec] so as to fit the initial part of the decay. The data are seen to vary in a very nearly Gaussian manner. This is undoubtedly accidental. Equation (23) corresponds to a slightly narrower homogeneous line than the data would in-

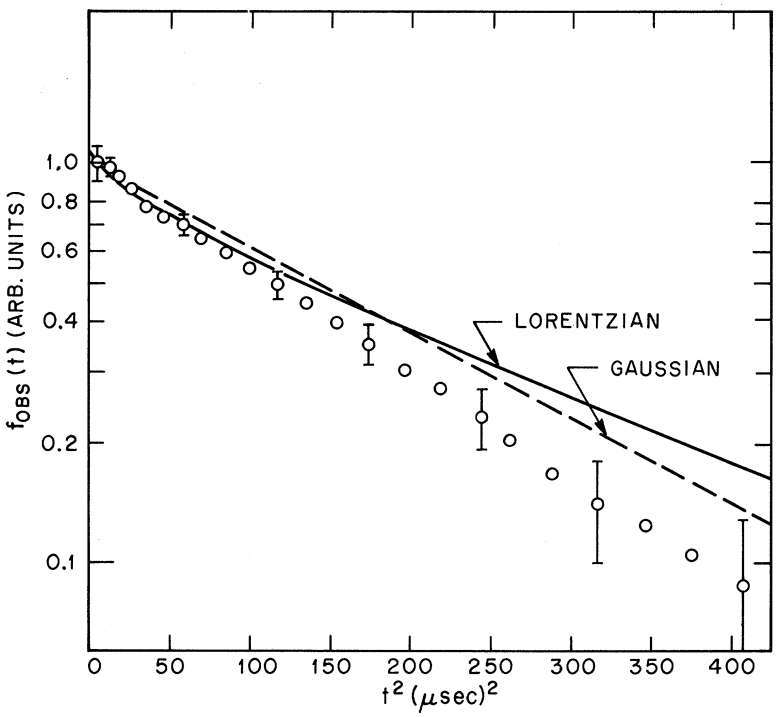

FIG. 3. Semilogarithmic plot of measured free-induction signal in zero applied field of ^{19}F in MnF_2 at 4.2 °K as a function of t^2. rf pulse width was 2 μsec. Curves plotted are described in text.

dicate, the error in T_2 (i.e., the e^{-1} point) being less than 15%. A simplified analysis has also been carried out assuming $g(h)$ to be Gaussian, resulting in a function $f_{obs}(t)$ that is then purely Gaussian. The width parameter for $g(h)$ is obtained simply from $m(0) = 0.36$, with the result for $f_{obs}(t)$ plotted as a dashed line in Fig. 3. No marked difference is observed between the two cases.

In discussing the experimental fit to these data one must also include some broadening effect due to the ^{55}Mn spins, i.e., by including a factor $e^{-t/T_2^{IS}}$ in the decay function [see Eq. (14)]. Although the estimate obtained earlier [Eq. (17)] would make only a relatively slight improvement in the fit, the truncated-Lorentzian model calculation may overestimate[16] T_2^{IS} by a factor as great as 2.5. Were this the case (e.g., $T_2^{IS} < 150$ μsec), we would at least find T_2 within experimental error.

In view of the simplicity of the Gaussian model and the uncertainties in determining $g(h)$, the agreement found here is considered satisfactory. The observed free-induction signal is seen to correspond, if anything, to a slightly broader line than the second moment indicates. There is clearly an absence of narrowing, and in fact good evidence for the correctness of the line-shape formulation of Sec. III.

V. CONCLUSIONS AND DISCUSSION: ECHO DECAY

The reformulation of unlike-spin broadening given in Sec. III has been seen to give a good account of the ^{19}F linewidth in antiferromagnetic MnF_2, where the narrowing effects implied by the moment technique are clearly absent. Presumably a line-shape measurement by steady-state methods would give a similar result. This would provide a useful confirmation of the present work. What remains to be understood is the spin-echo decay.

In contrast with the free-induction result of Sec. IV, the spin-echo decay has been found to be very nearly exponential with a somewhat longer decay constant (~ 30 μsec).[6] It is difficult to say whether this is or is not consistent with the present measurements. On this question we make the following observations including some qualitative experimental results:

(i) The echo measurements of Ref. 6 establish the exponential character of the decay only for times of order T_2 and greater, which is insufficient to characterize the line as "narrowed." Only if experiment shows that the exponential character extends to the $t \ll T_2$ region can the line reasonably be said to be narrowed.

(ii) It is difficult to account for the exponential character of the echo decay in the absence, as we have demonstrated here, of narrowing effects. The only line-shape theory which predicts long-time exponential free-induction behavior is the model calculation of Anderson and Weiss[24]; experimental evidence suggests that this type of behavior is the exception rather than the rule.

(iii) Because of the unavoidable presence of inhomogeneous broadening in MnF_2, it is difficult to rule out the possibility that long-time echo response is due to nuclei "detuned" from their neighbors and thus not subject to dynamic relaxation processes. This contrasts with free-induction response, where long-time behavior comes from spins in the center of the line.

(iv) As noted in the Introduction, the "moments"[8] of the echo decay vary with the pulse angle θ in a $\frac{1}{2}\pi$-θ echo sequence. Although a firm conclusion cannot be drawn from the second moment alone, it is possible that the general character of the decay may also vary with θ. There is a well-known theorem, valid for a single species of nucleus with long-range inhomogeneities, that the $\frac{1}{2}\pi$-π spin-echo decay is identical to the free-induction decay of the corresponding homogeneous system. It is straightforward to show that this correspondence also holds for the present case of two quasi-unlike ^{19}F species in MnF_2. Thus a careful measurement of the $\frac{1}{2}\pi$-π echo decay function should provide the same information as the experiments of Sec. IV.

There are, however, severe practical difficulties in carrying out such a measurement. First, in order to measure the echo response at short times, the line must be artificially dehomogenized to make $T_2^* \ll T_2$. It then becomes quite difficult to obtain a uniform π-pulse condition over the entire linebreadth as this requires $\gamma H_1 \gg 1/T_2^*$. Thus the initial flat region of echo decay ($t \ll T_2$), which is essential to the decay measurement, is beyond the reach of even a relatively high-power pulse rig.

One can carry out the measurement without external inhomogeneity and account for the interference effect between echo and free-induction signal as carefully as possible. Such a measurement has been performed, allowing some qualitative conclusions to be drawn about the echo decay as a function of θ for $t > T_2$. Pulses were applied with a 10-kW pulsed oscillator, achieving a 3-μsec π-pulse condition on a 1-cm^3 sample.[25] Echo response was observed for $\theta = \frac{1}{2}\pi$ and π and for the line severely dehomogenized with θ adjusted to give the best response. The last conditions are thought to correspond roughly to the measurements of Ref. 6. The following pattern of behavior was observed: With $\theta = \pi$ the echo was almost unobservable, reflecting a close similarity of echo-decay and free-induction function. At $t = 50$ μsec, this echo was at most ~3% of the initial free-induction amplitude. The $\frac{1}{2}\pi$-$\frac{1}{2}\pi$ echo was definitely larger and easier to observe, suggesting that its decay time is indeed longer than for $\frac{1}{2}\pi$-π in accord with the moment behavior. This effect is even more striking because the initial amplitude is only half that of the $\frac{1}{2}\pi$-π echo. Most interesting, perhaps, is the fact that the *largest* echo for $t > 2T_2$ was obtained by dehomogenizing the line with an external field and optimizing the pulses. Such an echo has the smallest initial value because of the wide range of pulse angles, yet it was found to be easily observable for $t > 100$ μsec. This effect was too clear cut to result simply from the loss of $I^{\pm}I'^{\pm}$ terms from the spin-spin Hamiltonian.[17]

Under the condition of a strong dehomogenizing field, then, it appears that the echo decay becomes longer than for "clean" $\frac{1}{2}\pi$-$\frac{1}{2}\pi$ or $\frac{1}{2}\pi$-π pulse sequences. Apart from the possibility of item (iii) above, this behavior is difficult to account for. In any case it seems unlikely that such an echo-decay time (i.e., the results of Ref. 6) is directly comparable with free-induction measurements. As noted above, the most appropriate comparison is between free induction and $\frac{1}{2}\pi$-π echo decay; the latter, being the shortest echo-decay time, is thought to be consistent with the measurements and conclusions of Sec. IV.

ACKNOWLEDGMENTS

The author wishes to thank Dr. M. Bulter and Dr. V. Jaccarino for several stimulating conversations as well as helpful comments on this manuscript, and Dr. L. R. Walker for his generous help and advice in the use of the results of Ref. 18. The technical assistance of A. Rodriguez is gratefully acknowledged.

APPENDIX

The Suhl-Nakamura coupling is derived[4,5] by calculating the second-order perturbation energy of the (^{19}F) hyperfine coupling, summed over intermediate states in which one spin wave is excited. For the ^{19}F hyperfine coupling we adopt the experimentally determined hyperfine tensor components for $ZnF_2:Mn^{2+}$,[19] as these are in close agreement with NMR results for MnF_2 where comparison is possible. Referring to Fig. 4, we associate with each up-spin Mn^{2+} site (j, for example) the two nearest ^{19}F nuclear spins. All spins in a given set of "like" ^{19}F's are accounted for in this fashion. Each set may be further divided into two simple tetragonal lattices [i.e., (A) and (B)], identical to that of the *up-spin* Mn^{2+}, but displaced along the (110) direction. The hyperfine coupling tensor for ^{19}F nucleus $j(A)$ may then be written

$$\mathcal{H}_{hf} = I^x_{j(A)}\left[A^{II}_{XX}S^x_j + A^I_{YY}(S^x_{j1} + S^x_{j2})\right] + I^y_{j(A)}\left[A^{II}_{YY}S^y_j + A^I_{XX}(S^y_{j1} + S^y_{j2})\right]. \quad \text{(A1)}$$

In (A1), the x axis is in the (110) plane of Fig. 1(a), the y axis is normal to the plane of the figure, and the z axis is along the (vertical) c axis of the crystal. The Mn^{2+} spin operator $\vec{S}_j$ is associated with site j and operators $\vec{S}_{j1}$ and $\vec{S}_{j2}$ are associated with sites displaced from j by vectors $\vec{\rho}_1$ and $\vec{\rho}_2$ (see

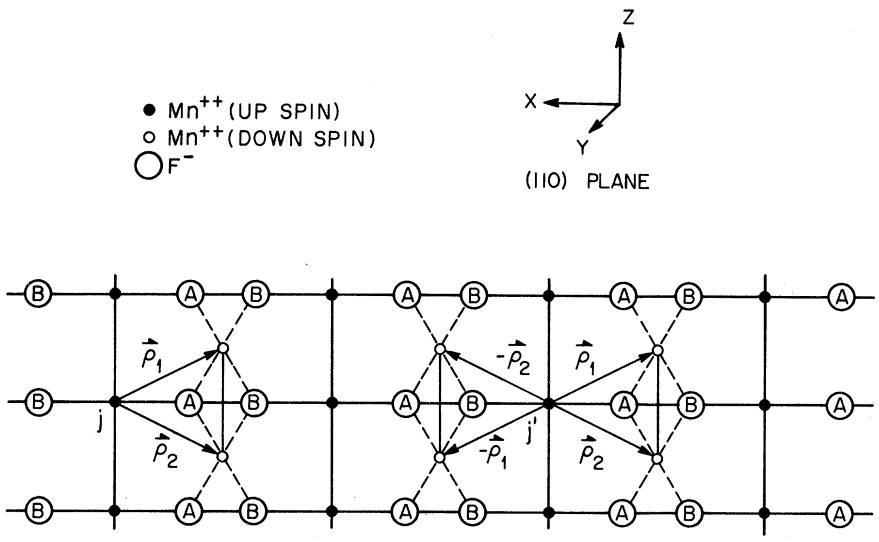

FIG. 4. (110) plane of MnF_2 (rutile) crystal structure, showing Mn^{2+} sites and associated F^- ions. "Like" ^{19}F nuclei are embedded in parallel sets of such planes, and are divided into groups A and B, each group forming a simple tetragonal lattice identical to, but displaced from, that of the (up-spin) Mn^{2+} sublattice.

figure), respectively. For the A coefficients, the notation from Ref. 19 is adopted in order to make use of the numerical values quoted there. Thus, $A^{I,II}_{XX}$ and $A^{I,II}_{YY}$ refer to X and Y axes defined in Ref. 19. The A^{I}_{YZ} coupling terms are omitted here, because they are not relevant to the SN interaction calculation.

Equation (A1) may be rewritten in terms of raising and lowering operators as

$$\mathcal{H}_{hf} = \tfrac{1}{2} I^{+}_{j(A)} [a^{II} S^{-}_{j} + a^{I}(S^{-}_{j1} + S^{-}_{j2}) + b^{II} S^{+}_{j} - b^{I}(S^{+}_{j1} + S^{+}_{j2})] + \tfrac{1}{2} I^{-}_{j(A)} [a^{II} S^{+}_{j} + a^{I}(S^{+}_{j1} + S^{+}_{j2}) + b^{II} S^{-}_{j} - b^{I}(S^{-}_{j1} + S^{-}_{j2})] , \quad \text{(A2)}$$

where

$$a^{I,II} = \tfrac{1}{2}(A^{I,II}_{XX} + A^{I,II}_{YY}) \quad \text{(A3)}$$

and

$$b^{I,II} S^{\pm}_{i} = \tfrac{1}{2}(A^{I,II}_{XX} - A^{I,II}_{YY}) .$$

The "normal" SN interaction energy consists of matrix-element products of the form $\langle 0 | S^{\pm}_{i} | k \rangle \times \langle k | S^{\mp}_{j} | 0 \rangle$, where $|0\rangle$ is the ground state and $|k\rangle$ is the state with one spin wave of wave vector k. From (A2), we see that the coefficients of such products will be either $(a^I)^2 + (b^I)^2$, $a^I a^{II} - b^I b^{II}$, or $(a^{II})^2 + (b^{II})^2$. These quantities as well as the hyperfine coefficients themselves from the work of Clogston *et al.*[19] are given in Table III. We note that the approximation of isotropic hyperfine coupling (in which $a^I = a^{II}$ and $b^I = b^{II} = 0$) is actually quite poor with the SN coefficients varying by nearly a factor of 2. Nevertheless, we proceed with this scheme in order to avoid an unwarranted increase in complexity in evaluating a small effect. Thus, we replace the three combinations in Table III with the average quantity $\langle a^2 \rangle_{av}$ as shown and expect the results to be accurate to perhaps ±25%. Equation (A2) then becomes

$$\mathcal{H}_{hf} \cong \tfrac{1}{2} \langle a^2 \rangle^{1/2}_{av} [I^{+}_{j(A)}(S^{-}_{j} + S^{-}_{j1} + S^{-}_{j2}) + I^{-}_{j(A)}(S^{+}_{j} + S^{+}_{j1} + S^{+}_{j2})] , \quad \text{(A4)}$$

where $\langle a^2 \rangle^{1/2}_{av}$ corresponds to the usual isotropic hyperfine coefficient A.

Before proceeding we note also from Eq. (A2) that the hyperfine anisotropy allows the presence of SN coupling term of the form $I^{\pm}_{j} I^{\pm}_{j'}$. For j and j' "unlike" these terms are secular in MnF_2 and thus contribute to the $M^{II'}_{2}(\pm\pm)$ second moment in Table II. A rough estimate of the magnitude of this effect is given below.

Beginning with (A4) we now follow Nakamura[5] in converting $\mathcal{H}_{hf}$ to spin-wave operators, evaluating the second-order perturbation energies and working out the second-moment contributions. The details of this process are straightforward and well known, so we shall only state the results. We note that one must distinguish carefully between the hyperfine

TABLE III. Hyperfine coupling parameters for ^{19}F in ZnF_2: Mn^{2+}, evaluated from data of Ref. 19. Quantities listed are defined in text.

a^I	13.7×10^{-4} cm^{-1}
a^{II}	18.4×10^{-4} cm^{-1}
b^I	-1.86×10^{-4} cm^{-1}
b^{II}	4.96×10^{-4} cm^{-1}
$(a^I)^2 + (b^I)^2$	1.908×10^{-6} cm^{-2}
$a^I a^{II} - b^I B^{II}$	2.612×10^{-6} cm^{-2}
$(a^{II})^2 + (b^{II})^2$	3.628×10^{-6} cm^{-2}
$\langle a^2 \rangle_{av}$	2.72×10^{-6} cm^{-2}

operators for ^{19}F nuclei at A and B sites in Fig. 4. This distinction was omitted in Refs. 5 and 7, leading to incorrect second-moment expressions. In terms of spin-wave operators, (A4) becomes

$$\mathcal{H}_{hf}=\left(\frac{S}{2N}\right)^{1/2}\langle a^2\rangle_{av}^{1/2}\Big(I^+_{j(A)}\sum_{\vec{k}} e^{-i\vec{k}\cdot\vec{R}_j}\{\alpha^*_{\vec{k}}[\cosh\theta_{\vec{k}}+\sinh\theta_{\vec{k}}\,(e^{-i\vec{k}\cdot\vec{\rho}_1}+e^{-i\vec{k}\cdot\vec{\rho}_2})]+\beta_{\vec{k}}[\sinh\theta_{\vec{k}}+\cosh\theta_{\vec{k}}\,(e^{-i\vec{k}\cdot\vec{\rho}_1}+e^{-i\vec{k}\cdot\vec{\rho}_2})]\}$$
$$+I^-_{j(A)}\sum_{\vec{k}} e^{i\vec{k}\cdot\vec{R}_j}\{\alpha_{\vec{k}}[\cosh\theta_{\vec{k}}+\sinh\theta_{\vec{k}}\,(e^{i\vec{k}\cdot\vec{\rho}_1}+e^{i\vec{k}\cdot\vec{\rho}_2})]+\beta^*_{\vec{k}}[\sinh\theta_{\vec{k}}+\cosh\theta_{\vec{k}}\,(e^{i\vec{k}\cdot\vec{\rho}_1}+e^{i\vec{k}\cdot\vec{\rho}_2})]\}\Big)\,. \tag{A5}$$

We emphasize that (A5) applies only to nuclei of type A in Fig. 4. The coupling with type-B nuclei is obtained by simply reversing the sign of $\vec{\rho}_1$ and $\vec{\rho}_2$ in (A5).

The SN coupling coefficients $D_{jj'}$ are defined in the usual way,[5]

$$\mathcal{H}_{SN}=-\tfrac{1}{2}\sum_{j>j'}(D_{jj'}I^+_jI^-_{j'}+D^*_{jj'}I^-_jI^+_{j'})\,, \tag{A6}$$

where we distinguish between A-A and A-B coupling coefficients with superscripts, i.e., $D^{AA}_{jj'}=D^{BB}_{jj'}$ and $D^{AB}_{jj'}\neq D^{BA}_{jj'}$. Equation (A5) then leads to Suhl-Nakamura energies

$$D^{AA}_{jj'}=\frac{\langle a^2\rangle_{av}}{zJN}\sum_{\vec{k}}\frac{e^{i\vec{k}\cdot(\vec{R}_j-\vec{R}_{j'})}}{x^2-\gamma^2}$$
$$\times[x(3+e^{i\vec{k}\cdot(\vec{\rho}_1-\vec{\rho}_2)}+e^{-i\vec{k}\cdot(\vec{\rho}_1-\vec{\rho}_2)})$$
$$-\gamma(e^{i\vec{k}\cdot\vec{\rho}_1}+e^{-i\vec{k}\cdot\vec{\rho}_1}+e^{i\vec{k}\cdot\vec{\rho}_2}+e^{-i\vec{k}\cdot\vec{\rho}_2})] \tag{A7}$$

and

$$D^{AB}_{jj'}=\frac{\langle a^2\rangle_{av}}{zJN}\sum_{\vec{k}}\frac{e^{i\vec{k}\cdot(\vec{R}_j-\vec{R}_{j'})}}{x^2-\gamma^2}\,[x(1+e^{2i\vec{k}\cdot\vec{\rho}_1}+e^{2i\vec{k}\cdot\vec{\rho}_2}$$
$$+2e^{i\vec{k}\cdot(\vec{\rho}_1+\vec{\rho}_2)})-2\gamma(e^{i\vec{k}\cdot\vec{\rho}_1}+e^{i\vec{k}\cdot\vec{\rho}_2})]\,. \tag{A8}$$

Here the magnon energy is taken to have the form $\epsilon_k=zJS(x^2-\gamma^2)^{1/2}$ with $x=1+\alpha$, where $\alpha=g\mu_BH_A/zJS$ is the ratio of anisotropy to exchange fields, and

$$\gamma(k)=z^{-1}\sum_{nn}e^{i\vec{k}\cdot\vec{r}_{nn}}\,.$$

Thus we employ the usual nearest-neighbor exchange model for the magnon excitations in MnF_2. Equation (A7) corresponds to Nakamura's Eq. (23a), but there is no counterpart to Eq. (A8) in previous literature.

With (A6) and the dipolar interaction Hamiltonian, it is straightforward to derive the following expressions for the Suhl-Nakamura and SN-dipolar (cross term) second moments:

$$M_2^{II}(\mathrm{SN})=\tfrac{1}{3}I(I+1)\Big(\sum_{j'(A)}{}'(D^{AA}_{jj'})^2+\sum_{j'(B)}(D^{AB}_{jj'})^2\Big)\,, \tag{A9}$$

$$M_2^{II}(\text{dipole-SN})=\gamma^2\hbar I(I+1)\Big(\sum_{j'(A)}{}'\frac{(1-3\cos^2\theta_{jj'})D^{AA}_{jj'}}{r^3_{jj'}}$$
$$+\sum_{j'(B)}\frac{(1-3\cos^2\theta_{jj'})D^{AB}_{jj'}}{r^3_{jj'}}\Big)\,, \tag{A10}$$

where the primed summation excludes the term $j'=j$. In order to evaluate (A9) and (A10) we make use of the tabulated spin-wave Green's function for the bcc lattice given by Walker, Cetlin, and Hone.[18] This is defined as

$$U(\epsilon,\vec{r})=\frac{1}{N}\lim_{\eta\to0^+}\sum_{\vec{k}}\frac{e^{i\vec{k}\cdot\vec{r}}}{(\epsilon+i\eta)^2-\epsilon^2_{\vec{k}}}\,. \tag{A11}$$

$U(\epsilon,\vec{r})$ is real for energies ϵ outside the magnon band and can be identified directly with the terms in $D^{AA}_{jj'}$ and $D^{AB}_{jj'}$ [(A7) and (A8)] for $x>1$. Furthermore, the terms in (A9) can all be written in terms of U and $U'=\partial U/\partial x$, where we make the substitution $x^2=(1+\alpha)^2-\epsilon^2$ in (A11). With this procedure the sums in (A9) are rewritten

$$\textstyle\sum'_{j'}(D^{AA}_{jj'})^2=(\langle a^2\rangle_{av}/zJ)\{(\frac{15}{2}x-2)\,U'(000)+(8x-\frac{13}{2})\,U'(100)$$
$$+(2x-7)\,U'(100)+(2x-\tfrac{5}{2})\,U'(111)+(x-\tfrac{1}{2})\,U'(200)-U'(210)$$
$$-\tfrac{1}{2}\,U'(211)+4[U(000)+U(100)+U(110)+U(111)]\}-(D^{AA}_{jj})^2 \tag{A12}$$

and

$$\textstyle\sum_{j'}(D^{AB}_{jj'})^2=(\langle a^2\rangle_{av}/zJ)^2\{(\frac{15}{2}x-2)\,U'(000)+(8x-\frac{13}{2})\,U'(100)$$
$$+(2x-7)\,U'(110)+(2x-\tfrac{5}{2})\,U'(111)+(x-\tfrac{1}{2})U'(200)-U'(210)$$
$$-\tfrac{1}{2}\,U'(211)+8[U(000)+U(100)]\}\,, \tag{A13}$$

TABLE IV. Interpolated values of $\partial U/\partial x$ at various lattice points for $x = 1.016$. Interpolation carried out as described in text.

Coordinates	$\frac{\partial U}{\partial x}$
(000)	4.145
(100)	2.679
(110)	2.304
(111)	2.061
(200)	1.786
(210)	1.650
(211)	1.530

where $U(a, b, c)$ stands for $U(x, \vec{p})$ with $\vec{p}$ as the lattice vector (a, b, c). The sums (A12) and (A13) are seen to be closely related, differing [apart from the self-term $(D_{jj}^{AA})^2$] by the quantity $4[U(000) + U(100) - U(110) - U(111)]$. This is easy to show directly with Eqs. (A7) and (A8) and provides a useful check on the results.

For numerical evaluation of the U's and U''s the value $x = 1.016$ ($\alpha = 0.016$) was adopted for MnF_2.[7] This choice is not critical as long as the spin-wave gap energy $\epsilon_g = (2\alpha)^{1/2} z_c JS$ is adjusted to have the experimental value $\epsilon_g/k_B = 12.54\,^\circ\mathrm{K}$.[26] The U's were evaluated by fitting the quantity[18] $\mathrm{Im}F(x) = xU(x)$ to a functional form[18]

$$\mathrm{Im}F(x) = \mathrm{Im}F(1) - (2/\pi)(x^2-1)^{1/2} + A(x^2-1) + B(x^2-1)^{3/2} \qquad \text{(A14)}$$

at $x = 1.012$ and 1.020. This procedure yielded an estimate of the quantity $A(x^2-1) + B(x^2-1)^{3/2}$ at $x = 1.016$ which was always within 0.1% of the value obtained from tabulated $F(x)$. The U''s were then obtained by differentiating (A14). The values of $U'(000)$ and $U'(100)$ so obtained were also compared with values obtained from the sum rules[18] using the other U''s, giving agreement within 0.2% or better.[27] The U''s resulting from the above procedures are stated in Table IV.

Using the U''s from Table IV and tabulated U''s in Ref. 18, we obtain the following results. Equation (A12) gives $\sum_{j'}' (D_{jj'}^{AA})^2 = 3.13$ with $(D_{jj}^{AA})^2 = 9.51$ and Eq. (A13) gives $\sum_{j'}(D_{jj'}^{AB})^2 = 7.83$, all in units of $(\langle a^2\rangle_{\mathrm{av}}/zJ)^2$. From (A9) we have $M_2^{II}(\mathrm{SN}) = 2.74$ $(\langle a^2\rangle_{\mathrm{av}}/zJ)^2$. Inserting the value of $\langle a^2\rangle_{\mathrm{av}}$ from Table III with J adjusted to give the correct spin-wave gap energy ($J = 3.51\,^\circ\mathrm{K}$) yields the value of $M_2^{II}(\mathrm{SN})$ in Table II. The numerical values of $\sum_{j'} (D_{jj'}^{AA})^2$ (= 12.64) and D_{jj}^{AA} given here are ~10% larger than the corresponding quantities given in Ref. 7, and the moment contribution $\sum_{j'} (D_{jj'}^{AA})^2 = 3.13$ from A-A coupling about 25% smaller. No effort has been made to resolve these discrepancies. We finally note that omitting the distinction between A-A and A-B coupling coefficients [(A7) and (A8)], as was done in previous treatments, results in a second moment ~50% larger than the value we give.

An estimate of the dipole-SN cross term (A10) was carried out by direct summation over the nearest 50 lattice sites using the tabulated Green's function[18] to evaluate $D_{jj'}^{AA}$ and $D_{jj'}^{AB}$. The parameters given in the previous paragraph lead to the value of M_2^{II}(dipole-SN) in Table II. The resulting tabulation of $D_{jj'}$'s also gave a useful check on the sums in (A9), accounting for ~90% of the calculated moment sum. This tabulation also forms the basis for the remarks in Sec. IV A on the nature of the ^{19}F-^{19}F SN interaction.

Lastly, we consider the SN coupling of the form $I_\pm^{(1)} I_\pm^{(2)}$ between unlike ^{19}F's, as described at the beginning of this Appendix. For a rough estimate of this effect, we consider only the coupling between nearest-neighbor "unlike" pairs. These share a common Mn^{2+} neighbor, and we calculate the SN coupling via this common neighbor only, neglecting the other eight interaction paths. The term we evaluate is expected, however, to predominate and give a reliable order-of-magnitude estimate.

The coupling operators for an unlike-neighbor pair are obtained straightforwardly from (A2) since one ^{19}F has type-I coupling and the other type-II:

$$\mathcal{H}_{\mathrm{hf}}^{(1)} = \tfrac{1}{2} b^I (I_+^{(1)} S_+ + I_-^{(1)} S_-) + \tfrac{1}{2} a^I (I_+^{(1)} S_- + I_-^{(1)} S_+) ,$$
$$\mathcal{H}_{\mathrm{hf}}^{(2)} = \tfrac{1}{2} b^{II} (I_+^{(2)} S_+ + I_-^{(2)} S_-) + \tfrac{1}{2} a^{II} (I_+^{(2)} S_- + I_-^{(2)} S_+) . \qquad \text{(A15)}$$

In (A15), $S_\pm$ are the transverse spin operators of the common Mn^{2+} neighbor. By the same procedures that led to (A7) and (A8) we then find for the coefficient of $I_+^{(1)} I_+^{(2)}$,

$$D_{nn}^{(+,+)} = +\tfrac{1}{2} \frac{(a^I b^{II} + a^{II} b^I)}{zJ} U(000) . \qquad \text{(A16)}$$

Taking the hyperfine couplings from Table III, J as given above, and $U(000) = -1.272$ from Ref. 18, we find $D_{nn}^{++} = -2.1 \times 10^3$ rad/sec. The magnitude of the corresponding dipolar coefficient is estimated to be 1.2×10^4 rad/sec, so that the SN effect is relatively minor. It is diminished considerably by a cancellation between the two terms in (A16). The relative phase of the SN and dipolar effects is such as to cause a net reduction in the coupling effect.

[1] J. H. Van Vleck, Phys. Rev. 74, 1168 (1948).
[2] A. Abragam and J. Winter, Compt. Rend. 249, 1633 (1959).
[3] See, C. P. Slichter, *Principles of Magnetic Resonance*

(Harper and Row, New York, 1963), Chap. 3, for a discussion of this question.

[4]H. Suhl, J. Phys. Radium 20, 333 (1959).

[5]T. Nakamura, Progr. Theoret. Phys. (Kyoto) 20, 542 (1958).

[6]N. Kaplan, P. Pincus, and V. Jaccarino, J. Appl. Phys. 37, 1239 (1966).

[7]D. Hone, V. Jaccarino, Tin Ngwe, and P. Pincus, Phys. Rev. 186, 291 (1969).

[8]Beginning with the well-known expression for the free-induction function in terms of the moments M_{2n} of a resonance line

$$f(t) = \sum_{n=0}^{\infty} \frac{(-1)^n M_{2n} t^{2n}}{(2n)!},$$

one may analogously define the "moments" of a spin-echo decay function $e(t)$, $M_{2n}^{(e)} = (-1)^n \, d^{2n}e(t)/dt^{2n}$. The quantities $M_{2n}^{(e)}$ are not "moments" in the sense of being weighted averages of an observable frequency distribution, and thus may be zero valued or negative.

[9]See, A. Abragam, *The Principles of Nuclear Magnetism* (Oxford U. P., Oxford, England, 1961), Chap. IV, for a discussion of the mathematical formulation of the method of moments.

[10]In the limit of rapid S-spin motion additional coupling terms, such as S^+I^+, will become effective in broadening the I resonance and will need to be included in (3).

[11]See Ref. 9, Chap. VIII, for a thorough review of these methods.

[12]The second and third terms in $\ln T$ represent the Zeeman splittings which are transformed out in going to the rotating frame.

[13]J. I. Kaplan [Bull. Am. Phys. Soc. 16, 338 (1971)] has recently discussed effects of lifetime broadening on the dipolar linewidth contribution, suggesting that the latter is reduced in magnitude when lifetime (i.e., T_2^{IS}) effects become important. Phenomena of this sort do not appear in the present calculation and are undoubtedly contained in higher-order expansion terms of the density-matrix equation of motion (9). It is interesting, however, that no such effect was observed in Ref. 15 (see discussion below).

[14]R. E. Walstedt, M. W. Dowley, E. L. Hahn, and C. Froidevaux, Phys. Rev. Letters 8, 406 (1962).

[15]J. Butterworth, Phys. Rev. Letters 8, 423 (1962).

[16]J. E. Gulley, B. G. Silbernagel, and V. Jaccarino, J. Appl. Phys. 40, 1318 (1969).

[17]D. Paquette, M. Butler, and V. Jaccarino, Phys. Rev. B 1, 160 (1970).

[18]L. R. Walker, B. B. Cetlin, and D. Hone, J. Phys. Chem. Solids 30, 923 (1969).

[19]A. M. Clogston, J. P. Gordon, V. Jaccarino, M. Peter, and L. R. Walker, Phys. Rev. 117, 1222 (1960).

[20]See Ref. 9, Chap. XII.

[21]$1/\tau^{IS}$ can be shown on the same thermodynamic arguments leading to Eq. (18) to be given by $(H_1^2/T^{IS} + H_L'^2/\tau_d^{IS}) \times (\Delta H^2 + H_1^2 + H_L'^2)^{-1}$, where τ_d^{IS} is the coupling time constant for the exchange of energy $\mathcal{H}_{II}$ with $\mathcal{H}_{SS}$. Since $H_1^2 \ll H_L'^2$, the measured τ^{IS} reflects primarily τ_d^{IS}. A small change in H_1 was found to make a noticeable difference in τ^{IS}, suggesting further that $\tau_d^{IS} \gg T_2^{IS}$ in accord with the estimate (17).

[22]V. Jaccarino and L. R. Walker, J. Phys. Radium 20, 341 (1959).

[23]M. H. Cohen and F. Reif, in *Solid State Physics*, edited by F. Seitz and D. Turnbull (Academic, New York, 1957), Vol. 5, p. 322.

[24]P. W. Anderson and P. R. Weiss, Rev. Mod. Phys. 25, 269 (1953).

[25]This could undoubtedly have been improved with smaller samples and better resonator design.

[26]F. M. Johnson and A. H. Nethercot, Jr., Phys. Rev. 114, 705 (1959).

[27]To obtain these accuracies it was necessary to refer to the original computer output for the tabulations in Ref. 18 for additional decimal places. The author wishes to thank L. R. Walker for providing access to these results.